Formulas for the Number of Surface Waves on Layered Structures

Guido Valerio, *Member, IEEE*, David R. Jackson, *Fellow, IEEE*, and Alessandro Galli, *Member, IEEE*

***Abstract*—Closed-form expressions are derived for the number of surface waves propagating along a general multilayered structure with media having positive material parameters. The expressions shown here are also useful for the efficient numerical determination and ordering of the cutoff frequencies of surface waves on multilayered structures. The presented formulas are simple but exact. Validation is provided with full-wave dispersive analyses of several types of layered structures.**

***Index Terms*—Dispersion analysis, layered media, surface waves.**

I. Introduction

LAYERED media are the constitutive elements of the most common structures in microwave and optical technology, from circuit [1] to antenna [2] applications, due to the availability of well-established manufacturing processes and analysis methods. The large variety of devices with layered media has further increased recently in the frame of the development of artificial media, often realized through periodic inclusions or perturbation in layered configurations [3], [4].

The design of all of these devices relies on effective analyses of the background structures, since their properties (e.g., the propagation of surface waves) heavily influence the behavior of the final components. Spurious excitation of surface waves can deteriorate performance because of coupling, edge diffraction from truncated substrates, and leakage of energy in the substrate [5], [6]. On the other hand, the correct analysis and design of many devices requires a careful study of the dispersive properties of the surface waves on the layers involved.

Very often, numerical analyses also require knowledge of the dispersive properties of arbitrary stratified structures. For example, in the formulation of integral equations and the computation of Green's functions [7], [8], the numerical efficiency can be enhanced by various kind of extractions [9]. In particular, the extraction of surface-wave contributions usually leads to fast-converging expressions and smoother results, thus significantly enhancing the effectiveness of the Sommerfeld integrations [10]. Furthermore, the regularized quantities are more easily interpolated through various techniques, e.g., polynomial approximations [11] or the complex image method [12].

Nevertheless, the numerical determination of surface-wave wavenumbers in general layered structures can be a difficult and time-consuming task, as the transcendental characteristic equation to be solved has both poles and zeros (the latter corresponding to the modal wavenumbers), possibly very near one to each other. The guided waves on a lossless layered structure with positive material parameters (i.e., for double-positive media) fall into three categories, which are: 1) *proper surface waves* (simply "surface waves" in the following), which have a real wavenumber and a proper field (exponentially decaying away from the structure); 2) *improper surface waves*, which have a real wavenumber and an improper field (exponentially increasing away from the structure); and 3) *leaky waves*, which have a complex wavenumber and an improper field. Various numerical approaches have been proposed for finding the complex wavenumbers (thus being applicable for leaky waves) [13], [14]. Some general properties of the surface waves have been proven in [15] for double-positive media, and these properties are useful for restricting the domain where the zero-searching is performed. In particular, it is proven there through a rigorous mathematical approach that the number of surface waves above cutoff is equal to the number of cutoff frequencies encountered while increasing the frequency from zero to the working frequency (some details that are relevant to the present paper are summarized in Section II).

In this paper, simple but rigorous closed-form expressions are found for the number of surface waves on a general lossless layered structure with double-positive media, in terms of the physical quantities involved (i.e., the thicknesses of the layers and their constituent parameters). This can be extremely important in developing effective zero searching algorithms of the relevant characteristic equation. The expressions discussed in this paper are also shown to be very useful for an effective numerical determination of the cutoff frequencies of any surface wave, thus providing information about the mode number ordering. A simple characterization is then possible, e.g., for the single-mode frequency range of the structure. Some results of these analyses have been briefly summarized in [16] without aim of completeness; the general formulation of the problem is explained and proven here in detail.

The method to obtain the required closed-form expressions is based on a modification of the well-known transverse-resonance-method approach [17]–[19]. A detailed description is given in the following sections. At first, general layered structures are considered; the presence of layers filled with media less dense than the denser unbounded medium requires a sep-

Manuscript received November 08, 2009; revised February 16, 2010; accepted March 04, 2010. Date of publication June 21, 2010; date of current version July 14, 2010.

G. Valerio and A. Galli are with the Department of Electronic Engineering, Sapienza University of Rome, 00184 Rome, Italy (e-mail: valerio@die.uniroma1.it; galli@die.uniroma1.it).

D. R. Jackson is with the Department of Electrical and Computer Engineering, University of Houston, Houston, TX 77204-4005 USA (e-mail: djackson@uh.edu).

Digital Object Identifier 10.1109/TMTT.2010.2050028

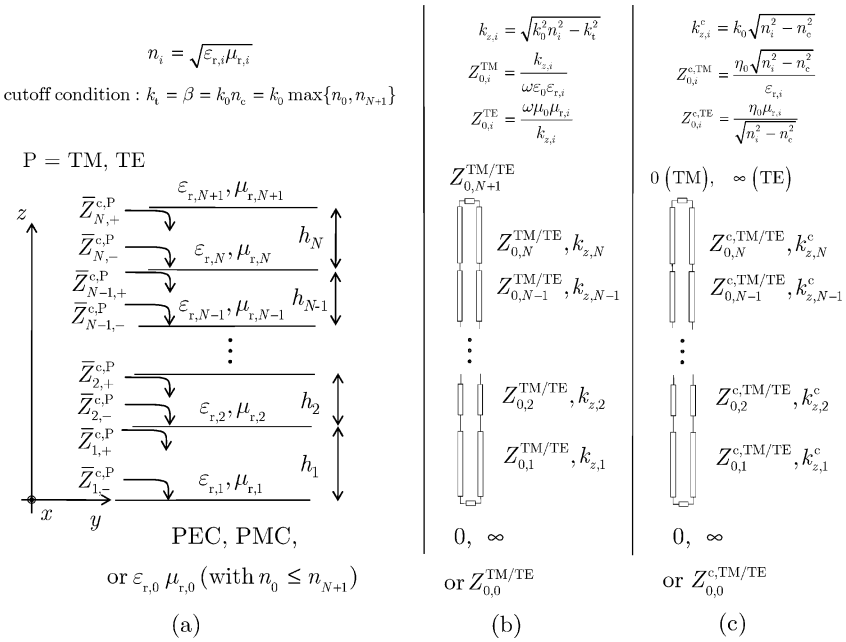

Fig. 1. (a) Diagram of a general layered structure analyzed in this work and relevant symbols. (b) Transmission line associated with the layered structure according to the transverse resonant technique, with constants as in (2) and (3). (c) Cutoff transmission line, with constants as in (4) and (5).

arate discussion and is treated later. Numerical results are presented to fully validate the new formulas and to show both the effectiveness and the generality of the method. The Appendix extends the formulas to the presence of uniaxially anisotropic media.

II. Method

A. General Discussion

A general lossless layered structure is considered as shown in Fig. 1(a) that is independent of the variables x and y ([20], [21]). An implicit time dependence $e^{j\omega t}$ is assumed. The structure consists of N homogeneous, isotropic, and nondispersive lossless layers; it is terminated at the bottom either with a perfect electric conductor (PEC), or with a perfect magnetic conductor (PMC), or an unbounded medium with parameters $\varepsilon_{\mathrm{r},0}, \mu_{\mathrm{r},0}$; at the top, it is terminated with an unbounded medium with parameters $\varepsilon_{\mathrm{r},N+1}, \mu_{\mathrm{r},N+1}$. Each layer has a refractive index $n_i = \sqrt{\varepsilon_{\mathrm{r},i}\mu_{\mathrm{r},i}} (i = 0, \ldots, N+1)$. In grounded (PEC/PMC) structures, the parameter n_0 is undefined.

The well-known transverse resonance technique can be applied to perform a modal analysis of the structure (see [17]–[19]). With this aim, a transverse equivalent transmission line can be introduced to describe the field dependence in the z direction (i.e., along the stratification), whose parameters are given in Fig. 1(b). This formalism allows one to perform modal analyses by solving the transcendental characteristic equation

$$\overleftarrow{Z}[\omega, k_{\mathrm{t}}(\omega)] = -\overrightarrow{Z}[\omega, k_{\mathrm{t}}(\omega)] \tag{1}$$

where $\overleftarrow{Z}$ and $\overrightarrow{Z}$ are the impedances seen looking downwards and upwards, respectively, at an arbitrary reference plane. Equation (1) is solved for the modal wavenumber k_{t} describing the propagation of a mode along any horizontal radial direction (which may be assumed to be the x-direction without loss of generality) as a function of the angular frequency ω.

In the complex k_{t} plane, the functions in (1) have branch points corresponding to the wavenumbers of the unbounded media on either side of the structure, so that its zeros can lie on different Riemann sheets. *Proper* zeros lie on the proper (top) sheet, where the radiation condition at infinity is satisfied in both the unbounded media and correspond to surface-wave modes of the structure. *Improper* zeros lie on the improper (bottom) sheet, where the fields exponentially increase in one or both of the unbounded regions and, hence, violate the boundary condition at infinity. These correspond to the leaky waves or to the improper surface-wave modes that evolve into leaky modes [22].

A *surface wave* is a mode whose wavenumber k_{t} is a proper real zero of (1), denoted in the following as β. The "standard" cutoff of a surface-wave mode corresponds to the crossing of an improper zero with a branch point; the zero crosses to the proper sheet and becomes a proper surface-wave mode of the structure as the frequency increases. If two unbounded media are present, the branch point of the denser medium defines the cutoff; the mathematical cutoff condition, at $\omega = \omega_{\mathrm{c}}$, is then $\beta = \omega_{\mathrm{c}} n_{\mathrm{c}}/c_0$, where $n_{\mathrm{c}} = \max\{n_0, n_{N+1}\}$ and $c_0 = 1/\sqrt{\mu_0\varepsilon_0}$. In a PEC or PMC grounded structure, with one unbounded upper medium, the same condition holds with $n_{\mathrm{c}} = n_{N+1}$.

As a preliminary basic consideration, it should be stressed that, at a given frequency, the number of surface waves above cutoff does not depend on the temporal dispersive behavior of the media; it depends only on the values of the media parameters at that frequency. To determine this number, a temporal-nondispersive structure can then be studied. In the following sections, the method will therefore be presented for temporal-nondispersive structures with no loss of generality.

All structures studied here are unbounded on at least one side and have lossless double-positive media, in order to apply some of the results from [15]. They can be summarized in three statements, which are: 1) $\beta(\omega)/k_0$ is always an increasing bounded function of ω; 2) no complex proper modes are solutions of (1); and 3) at low frequencies, the layered structure has the same dispersive properties as an effective single slab.

These properties imply that the number of surface waves at a given frequency f is then equal to the number of cutoffs that have occurred from zero frequency up to f. This would not be true if slabs with negative material parameters are considered (see, e.g., [23]). For instance, two surface waves could merge into a complex mode or plasmonic waves could exist that do not have a standard cutoff.

In this paper, the media is assumed to be lossless, and some comments regarding losses are therefore appropriate. If losses are present, then the wavenumber of a mode is always complex at any frequency. The trajectories of the relevant zeros of (1) in the complex $k_{\rm t}$ plane also change when loss is present; an improper (complex) zero becomes proper by crossing the Sommerfeld branch cut, rather than the branch point as in the lossless case [24]. The theoretical tools used in the following analysis (e.g., Foster's theorem and the fundamental properties outlined in [15]) rigorously hold for lossless structures only. Therefore, the formulas developed here (for the number of modes above cutoff) hold only for lossless structures. If small losses are present, the method presented here to derive the number of modes above cutoff is expected to remain valid, when cutoff is defined as the frequency for which the zero crosses the Sommerfeld branch cut, changing from an improper to a proper mode. For large losses, the method will not, in general, be valid. In this case the complex zeros of (1) must be studied for all of the modes in order to determine which modes are above cutoff.

Based on these statements, in the following subsections, closed-form expressions for the number of surface waves will be presented and discussed for different multilayered configurations. The presence of layers with media less dense than the denser of the two unbounded media is treated in a separate subsection, since some further considerations are necessary.

B. Closed-Form Expressions

Here, the closed-form expressions for the number of modes above cutoff are derived; the condition $n_i > n_{\rm c}$, for all $i = 1, \ldots, N$, will be assumed for the moment and relaxed later in Section II-C. If two unbounded media are present, $n_{N+1} \geq n_0$ is assumed with no loss of generality, thus $n_{\rm c} = n_{N+1}$. In grounded structures, this assumption is considered trivially verified since $n_{\rm c} = n_{N+1}$ always holds. As noted in Section II-A, a transverse equivalent network can be used to model each surface wave of the structure [see Fig. 1(b)]. The parameters depend on the type of mode (TM^z, i.e., $H_z \equiv 0$, or TE^z, i.e., $E_z \equiv 0$) as

$$k_{z,i}(\omega) = \sqrt{k_0^2 n_i^2 - \beta^2(\omega)} \tag{2}$$

$$Z_{0,i}^{\rm P}(\omega) = \begin{cases} \dfrac{\sqrt{k_0^2 n_i^2 - \beta^2(\omega)}}{\omega \varepsilon_0 \varepsilon_{{\rm r},i}}, & {\rm P} = {\rm TM} \\ \dfrac{\omega \mu_0 \mu_{{\rm r},i}}{\sqrt{k_0^2 n_i^2 - \beta^2(\omega)}}, & {\rm P} = {\rm TE} \end{cases} \tag{3}$$

where k_0 is the free-space wavenumber.

At cutoff, the TM impedance $\overrightarrow{Z}(\omega_{\rm c}) = 0$ and the TE admittance $\overrightarrow{Y}(\omega_{\rm c}) = 0$ at the uppermost interface. From the characteristic equation (1), at cutoff, also the TM impedance $\overleftarrow{Z}(\omega_{\rm c}) = 0$ and the TE admittance $\overleftarrow{Y}(\omega_{\rm c}) = 0$.

An auxiliary transmission line, referred to in the following as the "cutoff transmission line," can now be defined; the parameters (indicated with the superscript c) are obtained by replacing $\beta = k_0 n_{\rm c}$ in (2) and (3) [see Fig. 1(c)] so that

$$k_{z,i}^{\rm c}(\omega) = \frac{\omega}{c_0} \sqrt{n_i^2 - n_{\rm c}^2} \tag{4}$$

$$Z_{0,i}^{\rm c,P}(\omega) \equiv \begin{cases} \dfrac{\eta_0 \sqrt{n_i^2 - n_{\rm c}^2}}{\varepsilon_{{\rm r},i}}, & {\rm P} = {\rm TM} \\ \dfrac{\eta_0 \mu_{{\rm r},i}}{\sqrt{n_i^2 - n_{\rm c}^2}}, & {\rm P} = {\rm TE} \end{cases} \tag{5}$$

$\eta_0 = \sqrt{\mu_0/\varepsilon_0}$ being the free-space characteristic impedance. In PEC grounded structures $Z_{0,0}^{\rm c,P} = 0$, and in PMC grounded structures $Z_{0,0}^{\rm c,P} = \infty$; in both of these cases, (4) and (5) hold for $i \geq 1$. The parameters (4) and (5) are known in closed form since the wavenumber β of the surface wave is no longer present.

The normalized impedances seen *downwards* at the interface in the ith layer in the cutoff transmission line are indicated as $\bar{Z}_{i,\pm}^{\rm c,P}$. The bar denotes normalization with respect to the characteristic impedance of the ith layer; the $+(-)$ sign means that the impedance is measured at the top (bottom) of the ith layer, as shown in Fig. 1(a). The superscript "c" is a reminder that we are using the cutoff transmission-line parameters (4) and (5). Also, the reflection coefficient $S_{i,\pm}^{\rm c,P}$ associated with $\bar{Z}_{i,\pm}^{\rm c,P}$ will be defined as

$$S_{i,\pm}^{\rm c,P} = \frac{\bar{Z}_{i,\pm}^{\rm c,P} - 1}{\bar{Z}_{i,\pm}^{\rm c,P} + 1}. \tag{6}$$

Since $n_i > n_{N+1}$, all of the parameters in (4) and (5) are purely real and the cutoff transmission line models the propagation of a TEM wave along the z-axis; this corresponds to a cascade of N sections of multiconductor lines (e.g., parallel-plate waveguides or coaxial cables) filled with lossless double-positive media. The cutoff-transmission-line normalized impedance, looking down from the top interface, is then purely reactive, i.e., $\bar{Z}_{N,+}^{\rm c,P} = j\bar{X}_{N,+}^{\rm c,P}$. Moreover, from Foster's theorem [18], the reactance $X_{N,+}^{\rm c,P}$ is a monotonically increasing function of frequency [15]. Since all of the cutoff-transmission-line characteristic impedances are frequency-independent, the normalized reactance $\bar{X}_{N,+}^{\rm c,P}$ is monotonically increasing also.

Note also that, at a surface-wave cutoff, where $\omega = \omega_{\rm c}$ and $\beta = \omega_{\rm c} n_{\rm c}/c_0$, the parameters of the cutoff transmission line (4) and (5) are the same as the parameters of the transverse equivalent network (2) and (3). Accordingly, at cutoff, all of the impedances along the two lines assume the same values, and hence the cutoff conditions stated after (3) are valid also for the cutoff transmission line

$$\bar{Z}_{N,+}^{\rm c,TM} = 0 \quad \bar{Z}_{N,+}^{\rm c,TE} = \infty. \tag{7}$$

Each time the condition $\bar{X}_{N,+}^{\rm c,TM} = 0$ ($\bar{X}_{N,+}^{\rm c,TE} = \infty$) occurs, a new TM (TE) surface wave is at cutoff. Since, as explained in

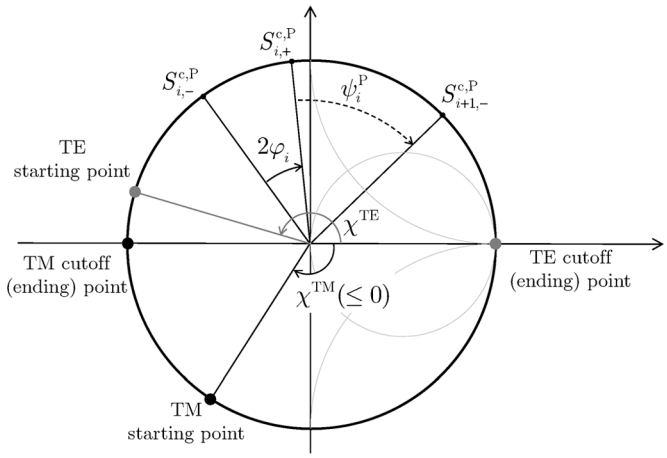

Fig. 2. Angles φ_i, ψ_i^{P}, and χ^{P} on the Smith chart.

Section II-A, the number of TM (TE) surface waves propagating at the frequency f is equal to the number of cutoff frequencies in the range from 0 to f, this number is given by the number of times $\bar{X}_{N,+}^{\mathrm{c,TM}}$ is zero ($\bar{X}_{N,+}^{\mathrm{c,TE}}$ is infinity) over this frequency range in the cutoff transmission line. A closed-form expression for this number will now be determined explicitly.

The value of $\bar{X}_{N,+}^{\mathrm{c,P}}$ can be iteratively calculated in closed form using simple transmission-line theory. The starting point of the algorithm depends on the medium at the bottom of the structure. If a PEC plane is present, $\bar{Z}_{1,-}^{\mathrm{c,P}} = 0$, and the starting point is the short-circuit point $(-1,\ 0)$ on a Smith chart. If a PMC plane is present, $\bar{Z}_{1,-}^{\mathrm{c,P}} = \infty$, and the starting point is the open-circuit point (1, 0). If an unbounded lower medium is present, the starting point depends on the polarization analyzed as follows:

$$\bar{X}_{1,-}^{\mathrm{c,TM}} = -\frac{\varepsilon_{\mathrm{r},1}\sqrt{n_{\mathrm{c}}^2 - n_0^2}}{\varepsilon_{\mathrm{r},0}\sqrt{n_1^2 - n_{\mathrm{c}}^2}} \quad \bar{X}_{1,-}^{\mathrm{c,TE}} = \frac{\mu_{\mathrm{r},0}\sqrt{n_1^2 - n_{\mathrm{c}}^2}}{\mu_{\mathrm{r},1}\sqrt{n_{\mathrm{c}}^2 - n_0^2}}. \tag{8}$$

The starting point can thus be easily placed in general on the Smith chart as shown in Fig. 2: it is determined by the angles $\chi^{\mathrm{P}} = \mathrm{Arg}\{S_{1,-}^{\mathrm{c,P}}\}$, where $S_{1,-}^{\mathrm{c,P}}$ is defined in (6). Note that $-\pi \leq \chi^{\mathrm{TM}} \leq 0$ and $0 \leq \chi^{\mathrm{TE}} \leq \pi$. The PEC termination can be included by letting $\chi^{\mathrm{TM}} = -\pi$ and $\chi^{\mathrm{TE}} = \pi$, and the PMC termination can be included by letting $\chi^{\mathrm{TM}} = \chi^{\mathrm{TE}} = 0$ (see Fig. 2 to visualize all the relevant angles).

After the starting impedance is computed, the recursive algorithm consists of the simple transmission-line formulas

$$\bar{X}_{i,+}^{\mathrm{c,P}} = \frac{\bar{X}_{i,-}^{\mathrm{c,P}}\cos\varphi_i + \sin\varphi_i}{\cos\varphi_i - \bar{X}_{i,-}^{\mathrm{c,P}}\sin\varphi_i} \tag{9}$$

$$\begin{aligned}\bar{Z}_{i+1,-}^{\mathrm{c,P}} &= j\bar{X}_{i+1,-}^{\mathrm{c,P}} \\ &= r_{i,i+1}^{\mathrm{c,P}}\bar{Z}_{i,+}^{\mathrm{c,P}} \\ &= jr_{i,i+1}^{\mathrm{c,P}}\bar{X}_{i,+}^{\mathrm{c,P}}\end{aligned} \tag{10}$$

where

$$\varphi_i = k_{z,i}^{\mathrm{c}} h_i \tag{11}$$

takes into account the phase shift along the ith layer and

$$r_{i,i+1}^{\mathrm{c,TM}} = \frac{Z_{0,i}^{\mathrm{c,TM}}}{Z_{0,i+1}^{\mathrm{c,TM}}} = \frac{\varepsilon_{\mathrm{r},i+1}\sqrt{n_i^2 - n_{\mathrm{c}}^2}}{\varepsilon_{\mathrm{r},i}\sqrt{n_{i+1}^2 - n_{\mathrm{c}}^2}} \tag{12}$$

$$r_{i,i+1}^{\mathrm{c,TE}} = \frac{Z_{0,i}^{\mathrm{c,TE}}}{Z_{0,i+1}^{\mathrm{c,TE}}} = \frac{\mu_{\mathrm{r},i}\sqrt{n_{i+1}^2 - n_{\mathrm{c}}^2}}{\mu_{\mathrm{r},i+1}\sqrt{n_i^2 - n_{\mathrm{c}}^2}} \tag{13}$$

take into account different impedance normalizations in different layers.

The iterative algorithm used to calculate $\bar{X}_{N,+}^{\mathrm{c,P}}$ can easily be visualized on the unit circle of the Smith chart (see again Fig. 2). Each layer corresponds to a clockwise rotation of $2\varphi_i$, while each crossing of an interface corresponds to a rotation of ψ_i, where

$$\psi_i^{\mathrm{P}} = \mathrm{Arg}\left\{S_{i+1,-}^{\mathrm{c,P}}\right\} - \mathrm{Arg}\left\{S_{i,+}^{\mathrm{c,P}}\right\} \tag{14}$$

and $\mathrm{Arg}\{x\}$ is the phase of the complex number x in $[-\pi, \pi)$. Since all r values are positive, $\bar{X}_{i,+}^{\mathrm{c,P}}$ and $\bar{X}_{i+1,-}^{\mathrm{c,P}} = r_{i,i+1}^{\mathrm{c,P}}\bar{X}_{i,+}^{\mathrm{c,P}}$ share the same sign. The determination of ψ_i^{P} is then chosen so that the path from the $S_{i,+}^{\mathrm{c,P}}$ point to the $S_{i+1,-}^{\mathrm{c,P}}$ point on the unit circle of the Smith chart does not cross the points (1, 0) and $(-1,$ 0) (this removes ambiguity in the calculation of phases).

Since $\bar{X}_{N,+}^{\mathrm{c,P}}$ monotonically increases with frequency according to Foster's theorem, the number of times $\bar{X}_{N,+}^{\mathrm{c,P}}$ crosses the cutoff point on the Smith chart is also the number of loops of $\bar{X}_{N,+}^{\mathrm{c,P}}$, starting from the point described above, and ending either at point $(-1,\ 0)$ for TM waves or at point (1, 0) for TE waves. This number of loops can be easily expressed through the above-defined angles $\varphi_i, \psi_i^{\mathrm{P}}, \chi^{\mathrm{P}}$.

Therefore, the number of TM surface waves above cutoff N^{TM} is

$$N^{\mathrm{TM}} = \mathrm{Floor}\left(\frac{A^{\mathrm{TM}}}{2\pi}\right) \tag{15}$$

where $\mathrm{Floor}(x)$ stands for the greatest integer less than x, and A^{TM} is the total angle swept by $\bar{X}_{N,+}^{\mathrm{c,TM}}$, expressed as

$$A^{\mathrm{TM}} = A_\varphi + A_\psi^{\mathrm{TM}} + A_{\mathrm{S}}^{\mathrm{TM}} \tag{16}$$

$$\begin{aligned}A_\varphi &= \sum_{i=1}^{N} 2\varphi_i \\ A_\psi^{\mathrm{TM}} &= \sum_{i=1}^{N-1} \psi_i^{\mathrm{TM}} \\ A_{\mathrm{S}}^{\mathrm{TM}} &= \pi - \chi^{\mathrm{TM}}\end{aligned} \tag{17}$$

where the angle $A_{\mathrm{S}}^{\mathrm{TM}}$ in (16) takes into account the starting point of the TM impedance at the bottom interface. In fact, when the angle $A_\varphi + A_\psi^{\mathrm{TM}} = \pi + \chi^{\mathrm{TM}}$, the first TM surface wave is at cutoff, since the point on the Smith chart crosses for the first time the point $(-1,\ 0)$.

Analogously, the number of TE surface waves above cutoff N^{TE} is equal to the number of times $\bar{X}^{\mathrm{c,TE}}_{N,+}$ crosses the point (1, 0), starting from the above-defined point, so that

$$N^{\mathrm{TE}} = \mathrm{Floor}\left(\frac{A^{\mathrm{TE}}}{2\pi}\right) \tag{18}$$

where A^{TE} is defined similarly as in (16), but

$$A^{\mathrm{TE}}_{\mathrm{S}} = 2\pi - \chi^{\mathrm{TE}}. \tag{19}$$

In fact, when the angle $A_\varphi + A^{\mathrm{TE}}_\psi = \chi^{\mathrm{TE}}$, the first TE surface wave is at cutoff, since the point on the Smith chart crosses for the first time the point (1, 0).

C. Case of Layers With $n_i < n_{\mathrm{c}}$

If layers less dense than the densest unbounded medium are present, i.e., the condition $n_i < n_{\mathrm{c}}$ holds for some i, the relevant $k^{\mathrm{c}}_{z,i}, \varphi_i$, and $Z^{\mathrm{c,P}}_{0,i}$ are imaginary. Some of the normalized impedances $\bar{Z}^{\mathrm{c,P}}_{i,\pm}$ are now real, and the corresponding points on the Smith chart lie on the real axis rather than on the unit circle.

In the following, $n_l < n_{\mathrm{c}}$, for $l = i+1, \ldots s$. The condition $s < N$ is assumed with no loss of generality, for the reason explained at the end of this section.

Since an attenuation occurs in these layers in the cutoff-transmission-line equivalent circuit, they are denoted in the following as "attenuated layers."

In the attenuated layers, the φ are imaginary and do not correspond to rotations on the Smith chart. The φ and ψ relative to the attenuated layers must then be set to zero in the expressions given above for N^{TM} and N^{TE}. Once the impedance comes back on the unit circle of the Smith chart, a ψ angle is determined according to the rule discussed in this section, between $S^{\mathrm{c,P}}_{i,+}$ (the last reflection coefficient on the unit circle) and $S^{\mathrm{c,P}}_{s+1,-}$ (the first reflection coefficient again on the unit circle).

The condition $k^{\mathrm{c}}_{z,l} = -j|k^{\mathrm{c}}_{z,l}|$ is assumed in the attenuated layers (i.e., if $i+1 \le l \le s$). This (arbitrary) choice grants an exponential decay of the reflection coefficient looking *downwards* when shifting along each layer in the *upward* direction. From (12) and (13), it then follows that

$$r^{\mathrm{c,TM}}_{i,i+1} = j\left|r^{\mathrm{c,TM}}_{i,i+1}\right| \tag{20}$$

$$r^{\mathrm{c,TE}}_{i,i+1} = -j\left|r^{\mathrm{c,TE}}_{i,i+1}\right| \tag{21}$$

$$r^{\mathrm{c,P}}_{l,l+1} > 0, \qquad \text{if } i < l < s \tag{22}$$

$$r^{\mathrm{c,TM}}_{s,s+1} = -j\left|r^{\mathrm{c,TM}}_{s,s+1}\right| \tag{23}$$

$$r^{\mathrm{c,TE}}_{s,s+1} = j\left|r^{\mathrm{c,TE}}_{s,s+1}\right|. \tag{24}$$

Since every real r in (22) is positive, the sign of the resistance along the line can change only because of the exponential damping of the reflection coefficient due to the shifts along the attenuated layers. It should be noted here that negative values of the normalized resistance are placed on the real axis on the Smith diagram, outside the unit circle.

The possible trajectories of the TM and TE impedances are shown in Fig. 3. For the sake of brevity, only the TM cases will explicitly be discussed in the following.

In Fig. 3(a), the case $\bar{X}^{\mathrm{c,TM}}_{i,+} < 0$ is treated. From (20), $\bar{Z}^{\mathrm{c,TM}}_{i+1,-} = r^{\mathrm{c,TM}}_{i,i+1}\bar{Z}^{\mathrm{c,TM}}_{i,+} = j|r^{\mathrm{c,TM}}_{i,i+1}|j\bar{X}^{\mathrm{c,TM}}_{i,+} > 0$. The exponential damping, therefore, cannot change the sign of the impedance, and thus $\bar{R}^{\mathrm{c,TM}}_{s,+} > 0$, and $j\bar{X}^{\mathrm{c,TM}}_{s+1,-} = r^{\mathrm{c,TM}}_{s,s+1}\bar{R}^{\mathrm{c,TM}}_{s,+} = -j|r^{\mathrm{c,TM}}_{s,s+1}|\bar{R}^{\mathrm{c,TM}}_{s,+}$. $\bar{X}^{\mathrm{c,TM}}_{s+1,-} < 0$ follows, as shown in the figure. The angle ψ must be calculated between the points $S^{\mathrm{c,TM}}_{i,+}$ and $S^{\mathrm{c,TM}}_{s+1,-}$. If only one attenuated layer is present, as its thickness tends to zero, the points $S^{\mathrm{c,TM}}_{i+1,-}$ and $S^{\mathrm{c,TM}}_{s,+}$ tend to coincide. Since, in this limit, we expect to get the same results obtained in the absence of the attenuated layer, the angle ψ must be taken between $S^{\mathrm{c,TM}}_{i,+}$ and $S^{\mathrm{c,TM}}_{s+1,-}$ in such a way that the path from $S^{\mathrm{c,TM}}_{i,+}$ and $S^{\mathrm{c,TM}}_{s+1,-}$ does not cross the $(-1, 0)$ and (1, 0) points.

In Fig. 3(b), the case $\bar{X}^{\mathrm{c,TM}}_{i,+} > 0$ is treated. From (20), $\bar{Z}^{\mathrm{c,TM}}_{i+1,-} = r^{\mathrm{c,TM}}_{i,i+1}\bar{Z}^{\mathrm{c,TM}}_{i,+} = j|r^{\mathrm{c,TM}}_{i,i+1}|j\bar{X}^{\mathrm{c,TM}}_{i,+} < 0$ (this normalized input resistance can have a magnitude either less than or greater than unity; Fig. 3(b) shows the latter case, where the corresponding point lies to the right of the (1,0) point). In this case, the exponential damping can change the sign of the impedance, by crossing the $(-1, 0)$ or the (1, 0) points. If it does not, a similar case to the one shown in Fig. 3(a) is found; ψ must be taken between $S^{\mathrm{c,TM}}_{i,+}$ and $S^{\mathrm{c,TM}}_{s+1,-}$ in such a way that the path from $S^{\mathrm{c,TM}}_{i,+}$ to $S^{\mathrm{c,TM}}_{s+1,-}$ does not cross either the $(-1, 0)$ or the (1, 0) points, as shown in Fig. 3(b).

In Fig. 3(c), the change in the sign of the normalized resistance due to the damping of the reflection coefficient is analyzed. If the thickness of the attenuated layer was sufficiently small, the case in Fig. 3(b) would occur and ψ would be chosen so that the path from $S^{\mathrm{c,TM}}_{i,+}$ to $S^{\mathrm{c,TM}}_{s+1,-}$ does not cross (1, 0). If the thickness is slightly increased, $S^{\mathrm{c,TM}}_{s,+}$ will coincide with the (1, 0) point, and thus $S^{\mathrm{c,TM}}_{s+1,-}$. ψ would then be the angle from $S^{\mathrm{c,TM}}_{i,+}$ to (1, 0), without crossing (1, 0). If the thickness is still increased, a change of the resistance sign occurs; by continuity ψ is the angle from $S^{\mathrm{c,TM}}_{i,+}$ to $S^{\mathrm{c,TM}}_{s+1,-}$, crossing the point (1, 0), as shown in the figure. A similar result would hold if the crossing occurs at the $(-1, 0)$ point.

The same analysis can be performed with reference to the TE polarization. It is omitted here for brevity, but it is described graphically in Fig. 3(d)–(f). As a final result, the general rule can be deduced. The angle ψ is determined so that the points (1, 0) and $(-1, 0)$ are never crossed, unless a change of the sign of the resistance occurs; if a change occurs, the angle ψ must cross the same point crossed by the resistance when it changed sign.

It is now possible to explain why the condition $s < N$ has been assumed at the beginning of this subsection. If $s = N$, the final normalized impedance $\bar{Z}^{\mathrm{c,P}}_{N,+}$ would be real; it would not be possible to calculate an angle ψ corresponding to the layers $i+1, \ldots, N$. In this case, a fictitious *auxiliary* layer can be added between the layer N and the unbounded medium $N+1$, with zero thickness and arbitrary refractive index $n_{\mathrm{aux}} > n_{\mathrm{c}}$. Since the thickness of this layer is null, the angle φ_{aux} is set to zero in the recursive calculation (9) and (10).

A final issue still needs to be discussed. In some sections of the cutoff transmission line, attenuation now occurs. The wavenumber is imaginary and linear with ω, and the characteristic impedance is imaginary and constant. Since this trans-

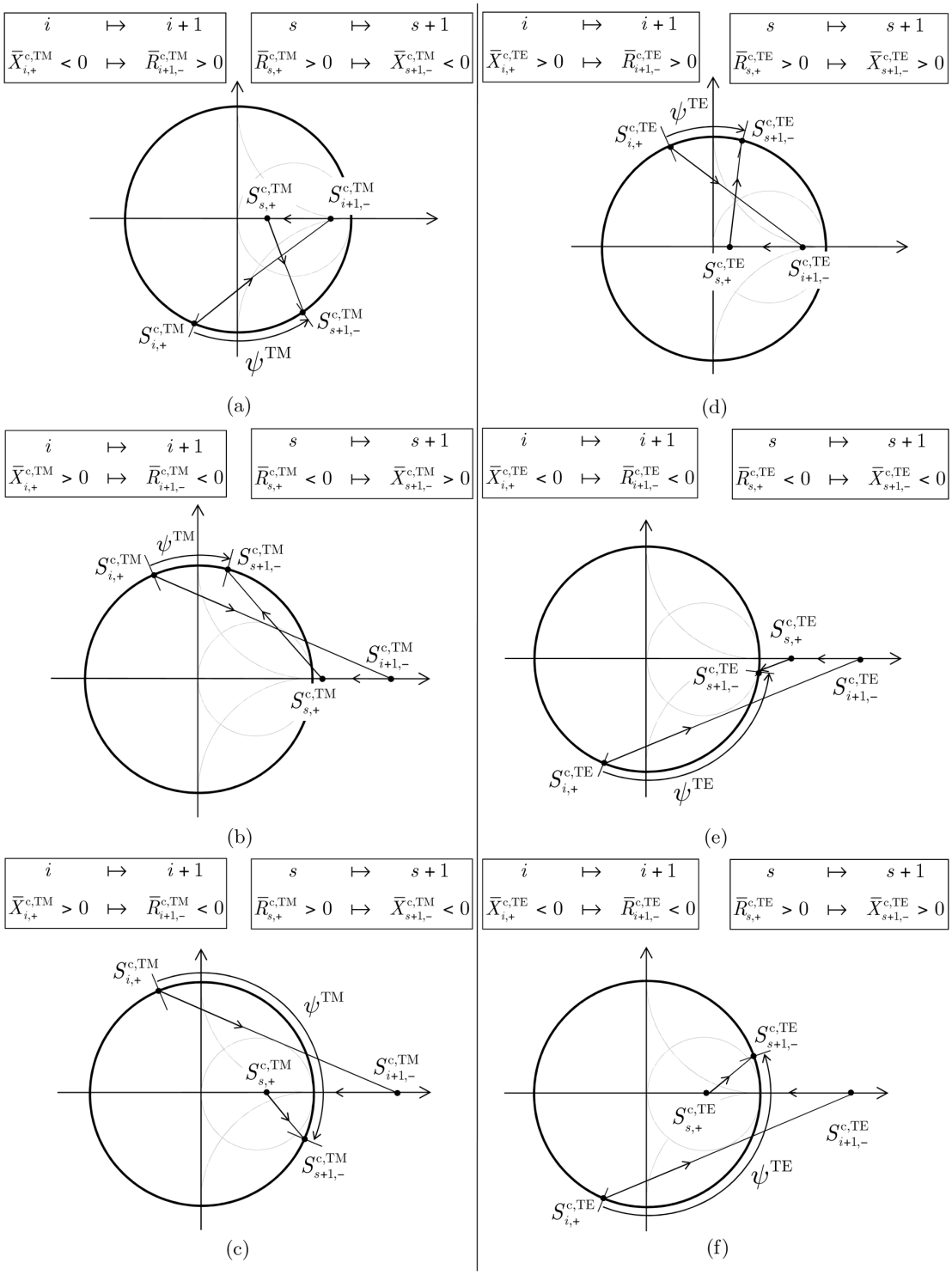

Fig. 3. Possible trajectories of the impedance on the Smith chart, with the correct choice of the angle ψ^{P} shown. The layers $i+1, \ldots, s-1, s$ are less dense than the denser unbounded medium. (a) TM impedance, $\bar{X}^{\mathrm{c,TM}}_{i,+} < 0$. (b) TM impedance, $\bar{X}^{\mathrm{c,TM}}_{i,+} > 0$. In (a) and (b), the normalized resistance does not change sign. (c) TM impedance, $\bar{X}^{\mathrm{c,TM}}_{i,+} > 0$, where the normalized resistance changes sign. (d) TE impedance, $\bar{X}^{\mathrm{c,TE}}_{i,+} > 0$. (e) TE impedance, $\bar{X}^{\mathrm{c,TE}}_{i,+} < 0$. In (d) and (e), the normalized resistance does not change sign; (f) TE impedance, $\bar{X}^{\mathrm{c,TE}}_{i,+} < 0$, where the normalized resistance changes sign.

mission line does not necessarily satisfy Foster's theorem [15], $\bar{X}^{\mathrm{c,TM}}_{N,+}$ can now be nonmonotonic with respect to ω. However, in [15], some weaker requirements for a monotonic behavior of the input impedance of such a line are proven. With reference to TM waves, we have

$$\frac{\partial X^{\mathrm{c,TM}}_{N,+}}{\partial \omega} > 0, \qquad \text{if } X^{\mathrm{c,TM}}_{N,+} \geq 0. \tag{25}$$

This inequality grants that the TM cutoff point at $(-1, 0)$ on the Smith chart can be crossed only from negative to positive values of the reactance, i.e., $X^{\mathrm{c,TM}}_{N,+}$ is monotonically increasing at the cutoff point. A similar result holds for TE waves

$$\frac{\partial X^{\mathrm{c,TE}}_{N,+}}{\partial \omega} > 0, \qquad \text{if } X^{\mathrm{c,TE}}_{N,+} \leq 0 \tag{26}$$

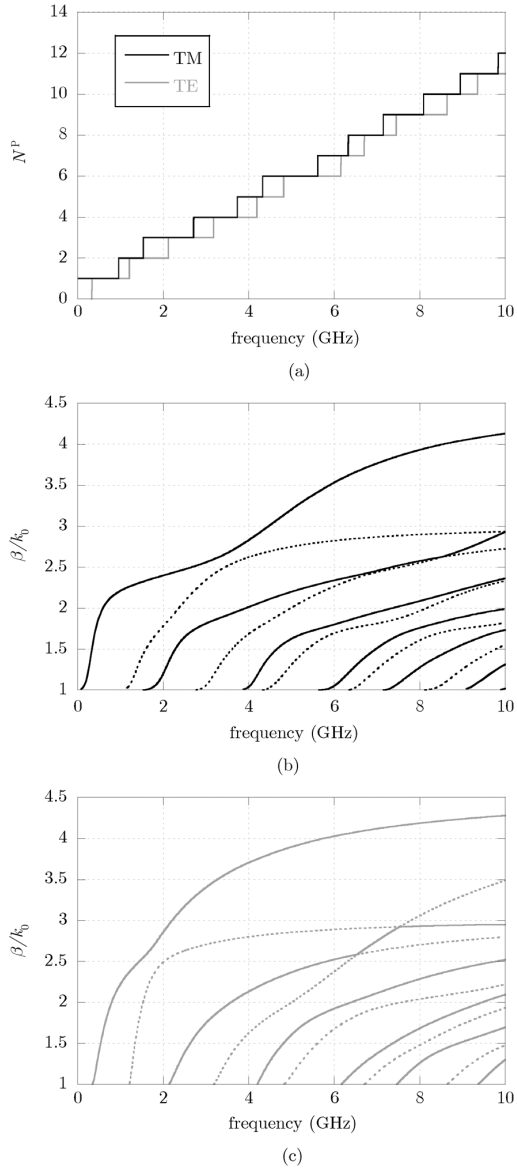

Fig. 4. Case of multilayer structure on a PEC. The structure has five layers with air on top with the following physical parameters: $h_1 = 15$ mm (0.05 λ_0 at $f = 1$ GHz, where λ_0 is the wavelength in vacuum), $h_2 = h_3 = h_1/2$, $h_4 = h_1$, $h_5 = 1.5h_1$, $\varepsilon_{\mathrm{r},1} = 2.2$, $\mu_{\mathrm{r},1} = 1.5$, $\varepsilon_{\mathrm{r},2} = 10.2$, $\mu_{\mathrm{r},2} = 2$, $\varepsilon_{\mathrm{r},3} = 2.2$, $\mu_{\mathrm{r},3} = 3$, $\varepsilon_{\mathrm{r},4} = 3$, $\mu_{\mathrm{r},4} = 1.4$, $\varepsilon_{\mathrm{r},5} = 9$, $\mu_{\mathrm{r},5} = 1$. (a) Number of TM (*black line*) and TE (*gray line*) surface waves according to (15) and (18), respectively. (b) Dispersion diagram of TM modes (*black solid lines* and *dotted lines*). (c) Dispersion diagram of TE modes (*gray solid lines* and *dotted lines*). In the dispersion plots, the line style used is different for adjacent modes to more clearly distinguish the curves.

granting that the TE cutoff point at (1, 0) on the Smith chart can be crossed only from positive to negative values of the reactance, i.e., $X^{\mathrm{c,TM}}_{N,+}$ is monotonically increasing at the cutoff point. This discussion ensures that the expressions found in the previous subsections hold in this case as well.

III. Numerical Calculation of Cutoff Frequencies

The closed-form expressions (15) and (18) for N^{P} (N^{TM} and N^{TE}) also allow for a simple evaluation of the cutoff frequencies of surface waves. Surface waves of the structure will be

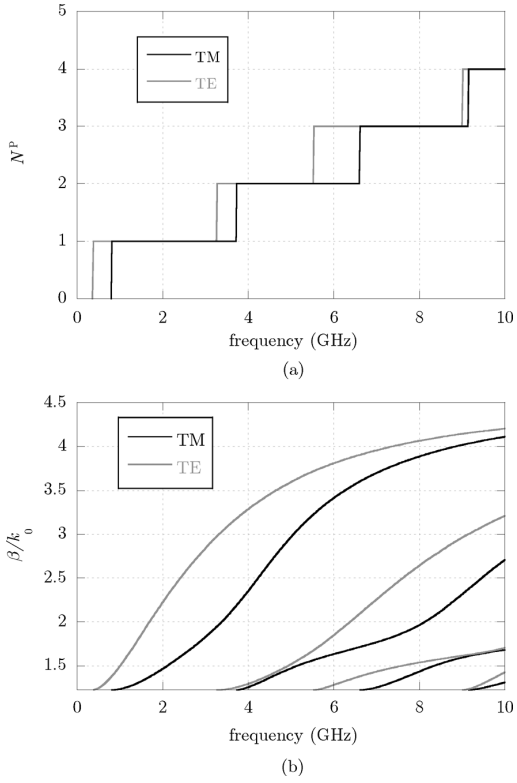

Fig. 5. Case of multilayer structure between two unbounded media ($n_i > n_{\mathrm{c}}$). A two-layer structure is terminated with air on the bottom, and with a medium ($\varepsilon_{\mathrm{r},3} = 1.5, \mu_{\mathrm{r},3} = 1$) at the top. Physical parameters of the two layers: h_1 =7.5 mm (0.025 λ_0 at $f = 1$ GHz), $h_2 = 2h_1, \varepsilon_{\mathrm{r},1} = 10.2, \mu_{\mathrm{r},1} = 2, \varepsilon_{\mathrm{r},2} = 2.2, \mu_{\mathrm{r},2} = 1.5$. (a) Number of TM (*black line*) and TE (*gray line*) surface waves according to (15) and (18), respectively. (b) Dispersion diagram of TM (*black lines*) and TE (*gray lines*) modes.

ordered with increasing cutoff frequencies and numbered with an integer index. For example, the TM_n mode is the nth TM mode of the structure when ordered with increasing cutoff frequencies.

If the cutoff frequency $f = f_{\mathrm{c}}$ of the TM_n or TE_n surface wave needs to be found, the following simple equation can be solved numerically with respect to the frequency, namely:

$$\frac{A^{\mathrm{P}}(f)}{2\pi} = n. \tag{27}$$

From the interpretation of A^{P} in terms of angles on the Smith chart, it is manifest that $A^{\mathrm{P}}(f)$, which can be easily calculated in closed form for any stratified structure, has no poles and that (27) has only one zero. Furthermore, in the cases treated in Section II-B, $A^{\mathrm{P}}(f)$ has a monotonic behavior (by Foster's theorem). These features make the numerical solution of (27) much more efficient with respect to the solution of the characteristic equation (1) at the cutoff condition $\beta = k_0 n_{\mathrm{c}}$, namely,

$$\overleftarrow{Z}\left(\omega_c, \frac{\omega_c}{c_0} n_{\mathrm{c}}\right) = -\overrightarrow{Z}\left(\omega_c, \frac{\omega_c}{c_0} n_{\mathrm{c}}\right). \tag{28}$$

In fact, the latter equation has also poles and cannot give information about the order of the mode found. In Section IV, some numerical results will show the effectiveness of solving (27) rather than the usual equation (28).

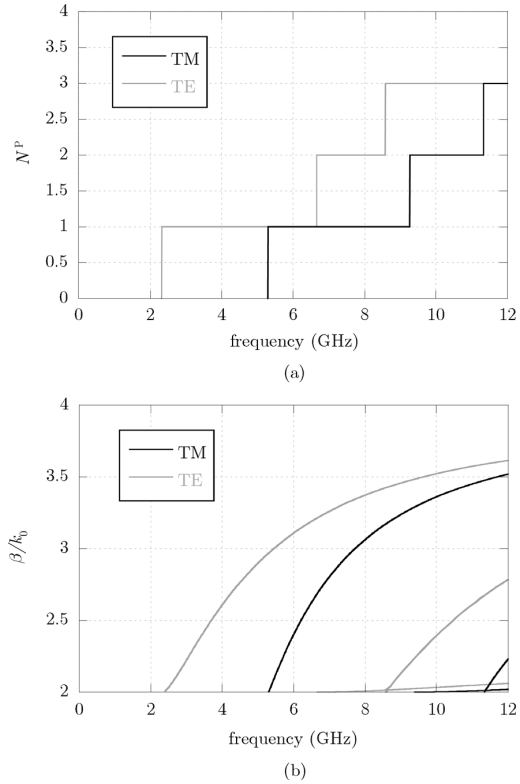

Fig. 6. Case of multilayer structure with an internal layer less dense than the densest unbounded medium. Three-layer structure terminated with air on the top, and with a different medium ($\varepsilon_{\mathrm{r},0} = 4, \mu_{\mathrm{r},0} = 1$) at the bottom. Physical parameters of the three layers: $h_1 = h_3 = 7.5$ mm, ($0.05\lambda_0$ at $f = 1$ GHz) $h_2 = 2h_1, \varepsilon_{\mathrm{r},1} = 5, \mu_{\mathrm{r},1} = 1, \varepsilon_{\mathrm{r},2} = 1, \mu_{\mathrm{r},2} = 1, \varepsilon_{\mathrm{r},3} = 10, \mu_{\mathrm{r},3} = 1.5$. (a) Number of TM (*black line*) and TE (*gray line*) surface waves according to (15) and (18), respectively. (b) Dispersion diagram of TM (*black lines*) and TE (*gray lines*) modes.

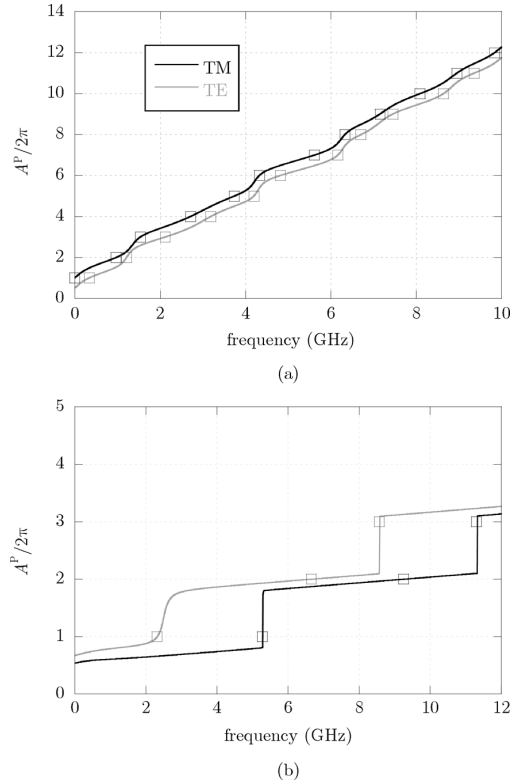

Fig. 7. Behavior of $A^{\mathrm{P}}(f)/2\pi$ for two of the structures previously analyzed, for the computation and ordering of cutoff frequencies. TM polarization (*black line*) and TE polarization (*gray line*). (a) Structure described in the caption of Fig. 4. (b) Structure described in the caption of Fig. 6.

IV. Numerical Results and Validation

Here, some numerical results will be presented to show the validity and usefulness of the method proposed in both determining the numbers of propagating surface waves and calculating cutoff frequencies.

A. Comparison With Known Closed Forms

If (15) and (18) are specialized in the simple case of a single grounded slab, the well-known expressions for the cutoff frequencies of the surface waves are found [18]. In fact, if $N = 1$, then

$$\frac{A^{\mathrm{TM}}}{2\pi} = n \Leftrightarrow \frac{2k_0\sqrt{n_1^2 - n_{\mathrm{c}}^2}h + 2\pi}{2\pi} = n$$
$$\Leftrightarrow \frac{h}{\lambda} = \frac{n-1}{2\sqrt{n_1^2 - n_{\mathrm{c}}^2}}, \qquad n = 1, 2, \ldots \tag{29}$$

and analogously for the TE modes. Known closed-form solutions can be obtained also with a PMC ground plane or a single slab bounded by air on both sides.

B. Comparison With Numerical Results for the Number of Surface Waves

As a first example, let us consider the case of a multilayered structure placed on a PEC ground plane (see Section II-B) with five internal slabs (Fig. 4). The number of TM and TE surface waves has been easily found through the closed-forms expressions (15) and (18) and is shown in Fig. 4(a). They agree with the dispersion analysis shown in 4(b) and (c) performed by numerically solving the characteristic equation (1) for both of the polarizations (β/k_0 is plotted with respect to the frequency). It is seen that the number of modes shown in Fig. 4(a) (predicted by the closed-form expressions) jumps by one at exactly the correct frequencies where a new mode emerges in the dispersion plots.

For the case of two different unbounded media with $n_i > n_{\mathrm{c}}$ (see again Section II-B), a two-layer structure is analyzed (Fig. 5). Results from the closed-form expressions shown in Fig. 5(a) are compared with a complete dispersion analysis of both TM and TE surface waves in Fig. 5(b). Again, full agreement was found.

Results for the case $n_i < n_{\mathrm{c}}$ (see Section II-C) are shown in Fig. 6: three layers are surrounded by two different unbounded media and the middle layer is air, which is less dense than the unbounded medium at the bottom of the structure. All the rules given in Section II-C are validated, since all of the possible cases (as described in Fig. 3) are present, depending on the frequency.

It is also interesting to note that, in the previous dispersion diagrams, some of the curves do not seem to be as smooth as might be expected, due to mode-coupling phenomena (see also [15]). The formulas derived here remain valid regardless of the level of mode coupling.

C. Numerical Calculation of Cutoff Frequencies

In Fig. 7(a), the left-hand side of (27) $A^{\mathrm{P}}(f)/2\pi$ is plotted with reference to the same structure and frequency range

analyzed in Fig. 4. $A^{\mathrm{P}}(f)$ is increasing with the frequency, as commented previously, according to Foster's theorem. Its smooth and regular behavior makes the numerical solution of (27) much easier with respect to the solution of (28), thus allowing a straightforward computation of the number of surface waves present at any frequency and their relevant cutoffs (see the squares in Fig. 7). In Fig. 7(b), the left-hand side of (27) is plotted for the same structure and frequency range analyzed in Fig. 6. Despite the fact that Foster's theorem does not apply to such a structure (as noted in Section II-C), in the case shown in the figure A^{P} is still monotonic; the solution of (27), which is still unique for a given n, is very simple when compared to the solution of (28).

V. Conclusion

Useful simple closed-form expressions for calculating the number of surface waves propagating along a general double-positive multilayered structure have been derived and discussed according to the different kind of parameters involved. All results are fully validated either with known closed-form expressions already available (for very simple geometries) or with rigorous dispersion diagrams obtained by numerically searching for the zeros of the relevant characteristic equations. An extension of the method to the numerical determination of the cutoff frequency of any surface wave is also illustrated, providing several advantages with respect to the usual method based on the solution of the characteristic equation at cutoff.

Appendix

The closed-form expressions derived here, in the case of isotropic layers, can be generalized to a layered structure composed of uniaxially anisotropic media with the optic axis along the stratification direction z, where

$$\underline{\boldsymbol{\varepsilon}}_i = \varepsilon_0 \begin{pmatrix} \varepsilon_{\mathrm{t},i} & 0 & 0 \\ 0 & \varepsilon_{\mathrm{t},i} & 0 \\ 0 & 0 & \varepsilon_{z,i} \end{pmatrix}$$
$$\underline{\boldsymbol{\mu}}_i = \mu_0 \begin{pmatrix} \mu_{\mathrm{t},i} & 0 & 0 \\ 0 & \mu_{\mathrm{t},i} & 0 \\ 0 & 0 & \mu_{z,i} \end{pmatrix}. \tag{30}$$

The transmission-line formulation in [19] can be used. The refractive indices are now

$$n_i^{\mathrm{TM}} = \sqrt{\mu_{\mathrm{t},i}\varepsilon_{z,i}} \quad n_i^{\mathrm{TE}} = \sqrt{\mu_{z,i}\varepsilon_{\mathrm{t},i}} \tag{31}$$

and the cutoff condition depends on the polarization of the mode since

$$n_{\mathrm{c}}^{\mathrm{P}} = \max\left\{n_0^{\mathrm{P}}, n_{N+1}^{\mathrm{P}}\right\}. \tag{32}$$

According to the formulation in [19], an appropriate definition of the cutoff-transmission-line parameters (4)–(5) should be chosen as

$$k_{z,i}^{\mathrm{c,P}}(\omega) = \frac{\omega}{c_0}\,\delta^{\mathrm{P}}\sqrt{\left(n_i^{\mathrm{P}}\right)^2 - \left(n_{\mathrm{c}}^{\mathrm{P}}\right)^2} \tag{33}$$

$$Z_{0,i}^{\mathrm{c,P}}(\omega) \equiv \begin{cases} \dfrac{\eta_0\sqrt{\left(n_i^{\mathrm{P}}\right)^2-\left(n_{\mathrm{c}}^{\mathrm{P}}\right)^2}}{\sqrt{\varepsilon_{\mathrm{t},i}\varepsilon_{z,i}}}, & \mathrm{P}=\mathrm{TM} \\ \dfrac{\eta_0\sqrt{\mu_{\mathrm{t},i}\mu_{z,i}}}{\sqrt{\left(n_i^{\mathrm{P}}\right)^2-\left(n_{\mathrm{c}}^{\mathrm{P}}\right)^2}}, & \mathrm{P}=\mathrm{TE} \end{cases} \tag{34}$$

with $\delta^{\mathrm{TM}} = \sqrt{\varepsilon_{\mathrm{t},i}/\varepsilon_{z,i}}$ and $\delta^{\mathrm{TE}} = \sqrt{\mu_{\mathrm{t},i}/\mu_{z,i}}$.

References

[1] D. M. Pozar, *Microwave Engineering*, 3rd ed. New York: Wiley, 2004.

[2] D. R. Jackson, "Microstrip Antennas," in *Antenna Engineering Handbook*, J. L. Volakis, Ed. New York: McGraw-Hill, 2007.

[3] P. S. Kildal, "Definition of artificially soft and hard surfaces for electromagnetic waves," *Electron. Lett.*, vol. 24, no. 3, pp. 168–1713, Feb. 1988.

[4] C. Caloz and T. Itoh, *Electromagnetic Metamaterials: Transmission Line Theory and Microwave Applications: The Engineering Approach*. Hoboken, NJ: Wiley, 2006.

[5] T. Tamir, "Inhomogeneous wave types at planar structures: I. The lateral wave," *Optik*, vol. 61, no. 5, pp. 209–232, Feb. 1972.

[6] F. Mesa and D. R. Jackson, "The danger of high-frequency spurious effects on wide microstrip line," *IEEE Trans. Microw. Theory Tech.*, vol. 50, no. 12, pp. 2679–2689, Dec. 2002.

[7] K. A. Michalski and D. Zheng, "Electromagnetic scattering by sources of arbitrary shape in layered media. Part I: Theory," *IEEE Trans. Antennas Propag.*, vol. 38, no. 3, pp. 335–344, Mar. 1990.

[8] K. A. Michalski and D. Zheng, "Electromagnetic scattering by sources of arbitrary shape in layered media. Part II: Implementation and results for contiguous half-spaces," *IEEE Trans. Antennas Propag.*, vol. 38, no. 3, pp. 345–352, Mar. 1990.

[9] G. Valerio, P. Baccarelli, S. Paulotto, F. Frezza, and A. Galli, "Regularization of mixed-potential layered-media Green's functions for efficient interpolation procedures in planar periodic structures," *IEEE Trans. Antennas Propag.*, vol. 57, no. 1, pp. 122–134, Jan. 2009.

[10] A. L. Fructos, R. R. Boix, R. Rodríguez-Berral, and F. Mesa, "Efficient determination of the poles and residues of spectral domain multilayered Green's functions that are relevant in far-field calculations," *IEEE Trans. Antennas Propag.*, vol. 58, no. 1, pp. 218–222, Jan. 2010.

[11] F. J. Demuynck, G. A. E. Vandenbosch, and A. R. Van de Capelle, "The expansion wave concept—Part I: Efficient calculation of spatial Green's functions in a stratified dielectric medium," *IEEE Trans. Antennas Propag.*, vol. 46, no. 3, pp. 397–406, Mar. 1998.

[12] M. I. Aksun, "A robust approach for the derivation of closed-form Green's functions," *IEEE Trans. Microw. Theory Tech.*, vol. 44, no. 5, pp. 651–658, May 1996.

[13] R. Rodriguez-Berral, F. Mesa, and F. Medina, "Systematic and efficient root finder for computing the modal spectrum of planar layered waveguides," *Int. J. RF. Microw. Comput.-Aided Eng.*, vol. 14, no. 1, pp. 73–83, May 2004.

[14] C.-I. G. Hsu, R. F. Harrington, J. R. Mautz, and T. K. Sarkar, "On the location of leaky wave poles for a grounded dielectric slab," *IEEE Trans. Microw. Theory Tech.*, vol. 39, no. 2, pp. 346–349, Feb. 1991.

[15] G. Valerio, D. R. Jackson, and A. Galli, "Fundamental properties of surface waves in lossless stratified structures," *Proc. R. Soc. A*, 2010, 24 pp.

[16] G. Valerio, A. Galli, and D. R. Jackson, "Properties of surface waves in general stratifed structures," in *Proc. URSI Nat. Radio Sci. Meeting*, Charleston, SC, Jun. 1–5, 2009.

[17] "Transverse Resonance Technique," in *Numerical Techniques for Microwave and Millimeter-Wave Passive Structures*, R. Sorrentino and T. Itoh, Eds. New York: Wiley, 1989.

[18] R. E. Collin, *Field Theory of Guided Waves*, 2nd ed. New York: IEEE, 1991.

[19] L. Felsen and N. Marcuvitz, *Radiation and Scattering of Waves*. New York: IEEE, 1991.

[20] G. W. Hanson and A. B. Yakovlev, *Operator Theory for Electromagnetics*. New York: Springer, 2001.

[21] W. C. Chew, *Waves and Fields in Inhomogeneous Media*. New York: Wiley, 1999.

[22] T. Tamir and A. A. Oliner, "The spectrum of electromagnetic waves guided by a plasma layer," *Proc. IEEE*, vol. 51, no. 2, pp. 317–332, Feb. 1963.

[23] P. Baccarelli, P. Burghignoli, F. Frezza, A. Galli, P. Lampariello, G. Lovat, and S. Paulotto, "Fundamental modal properties of surface waves on metamaterial grounded slabs," *IEEE Trans. Microw. Theory Tech.*, vol. 53, no. 4, pp. 1431–1442, Apr. 2005.

[24] R. Rodríguez-Berral, F. Mesa, A. L. Fructos, and R. R. Boix, "On the physical meaning of the spectral decomposition," *IEEE Microw. Wireless Compon. Lett.*, vol. 19, no. 8, pp. 488–490, Aug. 2009.

Guido Valerio (S'06–M'10) was born on May 29, 1982. He received the Master's degree (*cum laude* and honorable mention) in electronic engineering and Ph.D. degree in applied electromagnetics from Sapienza University of Rome, Rome, Italy, in 2005 and 2009, respectively.

In 2005, he joined the Electronic Engineering Department, Sapienza University of Rome, Rome, Italy, where he is currently an Associate Researcher. From February to August 2008 he was a Visiting Scholar with The University of Houston, Houston, TX. His scientific interests involve numerical methods for wave propagation and scattering in complex structures, such as periodic and multilayered media. Among other topics, he studies efficient computation and interpolation schemes for Green's functions pertaining to different kinds of periodic structures, the rigorous modeling of the interaction of nonperiodic sources with periodic media, and modal properties of both conventional and metamaterial multilayered structures. He is currently involved in the GPR characterization of Martian soil through both experimental and numerical approaches. He also works in the design of ultra-wideband antennas and harmonic-tunable active-antennas.

Dr. Valerio was the recipient of the Leopold B. Felsen Award for Excellence in Electrodynamics in 2008. In 2009, he was a finalist for the Young Engineers Prize at the European Microwave Conference.

David R. Jackson (F'99) was born in St. Louis, MO, on March 28, 1957. He received the the B.S.E.E. and M.S.E.E. degrees from the University of Missouri, Columbia, in 1979 and 1981, respectively, and the Ph.D. degree in electrical engineering from the University of California at Los Angeles (UCLA), in 1985.

From 1985 to 1991, he was an Assistant Professor with the Department of Electrical and Computer Engineering, University of Houston, Houston, TX, where, from 1991 to 1998, he was an Associate Professor and in 1998 became a Full Professor. He has served as an associate editor for *Radio Science* and the *International Journal of RF and Microwave Computer-Aided Engineering*. His present research interests include microstrip antennas and circuits, leaky-wave antennas, leakage and radiation effects in microwave integrated circuits, periodic structures, and electromagnetic compatibility and interference.

Dr. Jackson is presently serving as the chair of the Transnational Committee and the chair of the Distinguished Lecturer Committee of the IEEE Antennas and Propagation Society (AP-S) and as a Member-at-Large for U.S. Commission B of the International Union of Radio Science (URSI). He also serves as the chair of the MTT-15 (Microwave Field Theory) Technical Committee and is on the Editorial Board for the IEEE TRANSACTIONS ON MICROWAVE THEORY AND TECHNIQUES. Previously, he was the Chapter activities coordinator for the IEEE AP-S, a Distinguished Lecturer for the IEEE AP-S, an associate editor for the IEEE TRANSACTIONS ON ANTENNAS AND PROPAGATION, and a member of the Administrative Comittee (AdCom) for the IEEE AP-S. He has also served as the chair of U.S. Commission B of URSI.

Alessandro Galli (M'08) received the Laurea degree in electronic engineering and Ph.D. degree in applied electromagnetics from the Sapienza University of Rome, Rome, Italy.

In 1990, he joined the Electronic Engineering Department, Sapienza University of Rome, for research activities. In 2000 he became Assistant Professor and, in 2002, Associate Professor of Electromagnetic Fields. In his educational activities at Sapienza University of Rome, he is currently teaching the courses of "Electromagnetic Fields" and of "Applied Electromagnetics" for communications engineering. He is the author or coauthor of more than 200 scientific publications and of a patent for an invention concerning a new type of microwave antenna. He has worked on several projects and contracts involving universities, agencies, and industries, and has served in various capacities for institutional and professional activities. His scientific interests are focused on electromagnetic theory and applications in the main following research topics: microwave and millimeter-wave passive devices; scanning antennas and arrays; electromagnetic theory for waveguiding and radiating components, periodic structures, and metamaterials. He is also active in geophysical and in biological applications of electromagnetic fields.

Prof. Galli was elected as an Italian delegate on the Board of Directors of the European Microwave Association (EuMA) in 2010. He was the recipient of the Giorgio Barzilai Prize in 1994 for the best scientific work of under-35 researchers at the 10th National Meeting of Electromagnetics. He was also the recipient of the Quality Presentation Recognition Award by the IEEE Microwave Theory and Techniques Society (IEEE MTT-S) at the International Microwave Symposium in 1994 and in 1995.